Applied Catalysis B: Environmental 160–161 (2014) 335–343

Contents lists available at ScienceDirect

Applied Catalysis B: Environmental

journal homepage: www.elsevier.com/locate/apcatb

Understanding the storage function of a commercial NO*x*-storage-reduction material using operando IR under realistic conditions

Juliette Dupré[a], Philippe Bazin[a], Olivier Marie[a], Marco Daturi[a], Xavier Jeandel[b], Frédéric Meunier[a,c,*]

[a] Laboratoire Catalyse et Spectrochimie, ENSICAEN, Université de Caen, CNRS, 6 Bd Maréchal Juin, 14050 Caen, France
[b] Renault SAS, Engineering Mechanic Direction, FRCTL L47 2 61, 1 allée Cornuel, F-91510 Lardy, France
[c] Institut de Recherches sur la Catalyse et l'Environnement de Lyon, Université Lyon 1, CNRS. 2, Av. Albert Einstein, F-69626 Villeurbanne, France

ARTICLE INFO

Article history:
Received 14 February 2014
Received in revised form 26 April 2014
Accepted 18 May 2014
Available online 24 May 2014

Keywords:
NO*x*
Storage/reduction
Emission control
NO*x* trap
Operando IR spectroscopy

ABSTRACT

A thin self-supported wafer of a commercial NO*x*-Storage-Reduction (NSR) material was investigated by *operando* transmission FTIR to determine the nature of the surface and bulk species formed over the sample during the lean and rich cycles, while simultaneously monitoring the reaction cell effluent by on-line mass spectrometry and chemiluminescence. Conditions representatives of those found in catalytic converters were used, including large concentrations of water and CO_2. Water appeared to have a complex effect on NSR activity: on the one hand it hindered NO*x* storage and, on the other hand, it facilitated NO*x* reduction. Our data showed that both ionic and covalent carbonates were replaced by ionic and covalent nitrates when NO*x* were present. The large NO*x* uptake observed was mostly related to the replacement of ionic carbonates by ionic nitrates, mostly in the barium carbonate phase – but not in the bulk of large barium carbonate particles. The nitration of the bulk carbonate sites always remained low, i.e. <10% in all cases. It is possible that some other elements present (such as Mg, Ce, Sr, Cs) also contributed to some extent to the formation of the ionic species. The contribution of covalent species (e.g. formed on surface sites of alumina and ceria) to the storage was negligible, though some of those species could potentially be intermediates in the surface migration of ionic species. The trapping on hydroxyl sites was found to be negligible in the present case.

1. Introduction

Lean burn engines operating under an excess of oxygen (lean conditions) improve fuel efficiency and so reduce CO_2 emissions in comparison with stoichiometric engines. An end-of-the-pipe technology is yet required to treat the corresponding NO*x* emissions [1], such as the NO*x*-Storage-Reduction (NSR) technique initially introduced by Toyota [2]. A detailed description of the fundamentals of the NSR technology and a review of the activity of many materials has been reported elsewhere [3].

In brief, alternating lean and rich conditions are employed during engine operation, leading to oxidizing and reducing exhaust gases, respectively. The NO*x* are first retained on the NSR materials under lean conditions, before being reduced under rich conditions. An efficient NSR material should typically exhibit specific sites for NO*x* sorption (alkali metal or alkaline earth metal compounds, most often Ba) and sites for NO*x* oxidation/reduction (noble metals). The understanding of NSR technology has been hampered by the fact that various (usually non-realistic) reaction conditions were often used and a very large number of model materials with varying formulations were investigated [4–20].

The review by Roy and Baiker emphasized in particular that the nature of the Ba species involved in the trapping was yet unclear, e.g. an oxide or carbonate of Ba [3]. Nitrites were proposed to be first formed followed by nitrates. The direct role of the support in the storage function, by NO*x* spill-over, has also been raised. The authors also emphasized the discrepancy brought about by the use of simplified reaction feed that do not contain significant concentrations of water and CO_2 [3].

The combination of in situ IR spectroscopy (to determine the nature and concentration of sorbed species) and kinetic analysis of reaction cell effluents can be a powerful tool to unravel the

* Corresponding author at: Institut de Recherches sur la Catalyse et l'Environnement de Lyon, Université Lyon 1, CNRS. 2, Av. Albert Einstein, F-69626 Villeurbanne, France. Tel.: +33 4 72 44 54 68; fax: +33 4 72 44 53 65.
E-mail address: Frederic.meunier@ircelyon.univ-lyon1.fr (F. Meunier).

http://dx.doi.org/10.1016/j.apcatb.2014.05.027
0926-3373/

features of storage processes and catalytic reactions. The number of NSR studies combining simultaneous surface and gas-phase analysis over a single sample is yet low [21–28]. This observation may be partly due to the fact that the reaction cells to be used are complex and need to be custom-made or modified to provide kinetically relevant data [28–32].

Urakawa et al. used a custom-made cell combining DRIFT and Raman spectroscopies over a model Pt-Ba-CeO_2 NSR material [26]. This system enabled space- and time-resolved spectra with evolved effluent gas compositions. The accumulation of nitrate and nitrite species was shown to occur at the front of the converter bed. Yet, the use of diffuse reflectance induces difficulties in the precise quantification of the relevant species.

The results presented here were obtained using a NSR material extracted from a commercial NSR monolith supplied by Renault S.A.S. The surface and bulk species present on the solid (studied by *operando* FTIR spectroscopy under representative conditions, i.e. including water and CO_2) were monitored using a unique low-volume transmission IR cell. One benefit of the present method is that the entire sample volume was probed, contrary to the case of diffuse reflectance FTIR studies for which only the superficial layer of the sample bed is typically probed. The NSR efficiency (i.e. trapping and reduction of NO*x*) was simultaneously measured over the same sample using an on-line mass spectrometer, an IR gas-cell and a chemiluminescence. The effect of added water concentration and the role of bulk barium carbonates were investigated. The main goal of the study was to provide some insight into the nature of the species formed over the NSR material during the lean phase.

2. Experimental

A powder of the NSR material was detached from an oven-aged cordierite-based monolith supplied by Renault S.A.S. using an undisclosed method. The exact composition of the powder cannot be disclosed but Pt was the main noble metal (ca. 0.6 ± 0.5 wt.%), followed by Pd (ca. 0.2 ± 0.1 wt.%) and then Rh (ca. 0.1 ± 0.05 wt.%). As far as oxides were concerned, the main constituents were the following, in order of decreasing concentration: Al (ca. 25 ± 5 wt.%), Ce (ca. 15 ± 5 wt.%), Si (ca. 7 ± 3 wt.%), Mg (ca. 7 ± 3 wt.%), Ba (ca. 4 ± 2 wt.%), Zr (ca. 2 ± 1 wt.%), Fe (ca. 0.6 ± 0.4 wt.%), Sr (ca. 500 ± 300 wt.ppm) and Cs (ca. 700 ± 300 wt.ppm).

A schematic lay-out of the system is shown in Fig. 1. A custom-made low volume transmission *operando* cell fitted with KBr windows was used. The cell was manufactured by Aabspec International Ltd. following a design jointly developed with our laboratory and now commercially available as model n° CX. Detailed views of the Aabspec–CX IR reactor cell are reported by Bobadilla et al. [33]. For the surface analysis, the measurements were carried out in the transmission mode with a Nicolet 6700 FTIR spectrometer equipped with a MCT detector. FTIR spectra were collected with a resolution of 4 cm^{-1} using 6 or 32 scans per spectrum depending on the time resolution desired. The spectra were treated using the OMNIC® software. The analysis of the outlet gases was performed by means of a FTIR gas microcell (in particular to observe N_2O) and a Pfeiffer Omnistar mass spectrometer. A chemiluminescence cell (From ThermoScience, model 42i-HL) was also used for some experiments to precisely determine NO and NO_2 concentrations. In order to decrease the signal due to ambient H_2O and CO_2, the IR spectrometer and the sample compartment were purged with H_2O and CO_2-free air.

The samples were pressed into self-supporting wafers of about 10 mg cm^{-2}. Feed conditions representative of the emissions of a Euro 5 Diesel engine were used for the lean and rich phases. The compositions are given in Table 1. The presence of methane in the feed is unusual in the academic studies, but methane is usually present in the real exhaust flow measured on Renault S.A.S. engine benches. Methane and ethene together were reported elsewhere to account for 59% of total light hydrocarbons [34]. Methane formation was also generated during the ultra-high Exhaust Gas Recirculation (EGR) operation [35].

Table 1
Concentrations of gases in the base feed, to which was added either the lean or the rich feed.

Base feed	Rich feed	Lean feed
10% CO_2	750 ppm CH_4	100–180 ppm NO
1–4% water	2.17% CO	525 ppm CO
Ar balance	0.73% H_2	174 ppm H_2
	0.89% O_2	8.7% O_2
	5800 ppm C_3H_6	

The so-called "base" feed was always present in the gas stream sent to the reaction cell. The total flow-rate passing over the wafer was 25 ml/min. Note that the lean and the rich feeds were merged after the reaction cell and simultaneously analyzed, so that any NO*x* released during the rich phase could also be measured. Before applying the cycling NSR procedure, the sample was treated at 600 °C under the rich phase for 1 h and then the temperature was set to that of the experiment (i.e. 300 °C). The pre-treatment was intended to remove any traces of pollutants that may have contaminated the surface to ensure reproducible experiments from one day to the other and to facilitate the spectroscopic data interpretation. During the NSR cycles, the duration of the trapping period was 10 min and that of the regeneration period was 30 s. The cycling frequencies were established by Renault S.A.S. and corresponded to a precise operation in NO*x* removal, based on a fixed average efficiency on cars.

A computer-controlled automated 6-way valve (Swagelok) was used to complete the base feed with either the lean or rich feed to the reaction cell. The NSR material was typically stabilized over five full cycles before five other cycles were collected to calculate an averaged NSR activity. The NO*x* conversion was defined by the equation:

$$\text{NO}x\text{ conversion} = \frac{\text{NO fed} - \text{NO}x\text{ measured}}{\text{NO fed}} \quad (1)$$

where "NO fed" was the amount of NO introduced to the reactor over a full cycle and "NO*x* measured" was the amount of NO*x* (=NO + NO_2) measured also over a full cycle. The maximum achievable conversion was ca. 95% using this definition, as the NO-containing stream by-passed the reactor for 30 s over a total cycling period of 10.5 min. The nature of the reduction products was not investigated in details, but gas-phase IR analysis revealed significant proportions of N_2O, while no ammonia was observed (N_2 is not IR sensitive and cannot be resolved by MS studies in the presence of large concentrations of CO and CO_2). The fraction of NO*x* trapped over the lean period was also calculated using the same equation as that for the NO*x* conversion but only taking into account the NO fed and NO*x* in the cell effluent during the lean period:

$$\text{NO}x\text{ trapped} = \frac{\text{NO}x\text{ fed(lean)} - \text{NO}x\text{ measured(lean)}}{\text{NO fed(lean)}} \quad (2)$$

Note that the value of NO*x* trapped was usually greater than that of NO*x* conversion because not all the NO*x* trapped were reduced during the rich phase. The gas hourly space velocity (GHSV) used, based on the volume of NSR materials (free of cordierite support) were in the realistic range 45 000–100 000 h^{-1}, extrapolated from the conditions used during Renault S.A.S. tests.

The thermodynamic calculations were carried out using the HSC Chemistry software, © Outotec Research Oy, version 6.2.

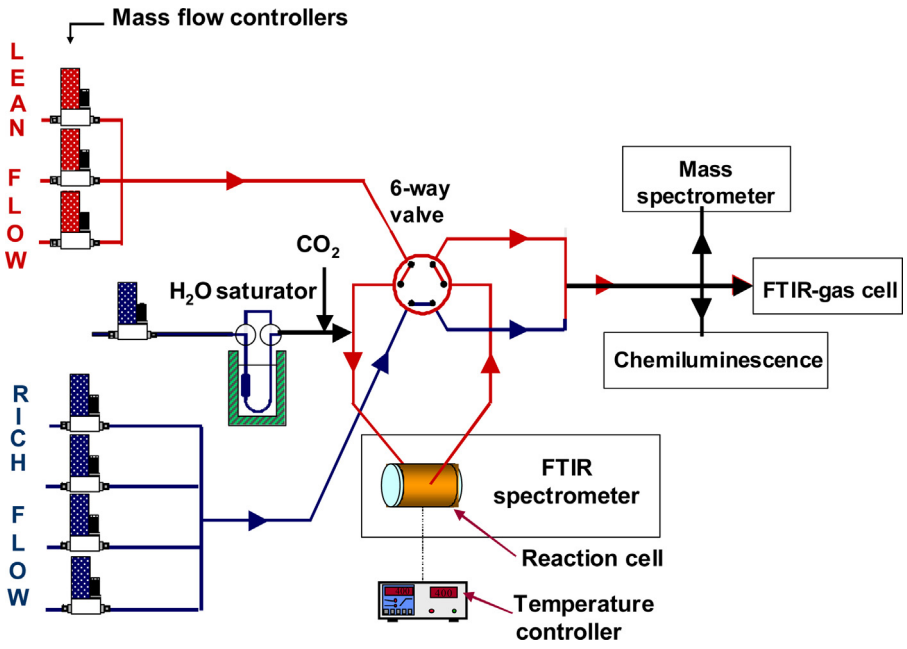

Fig. 1. Schematic representation of the experimental setup used for NO*x*-storage-reduction. The transmission IR reaction cell is located in a FTIR spectrometer and the corresponding reactor effluents are analyzed by mass spectrometry, gas-phase FTIR and chemiluminescence.

3. Results and discussion

3.1. Kinetic results

The analysis of the mass spectrometer (MS) signal is first discussed, since this technique was the one routinely used to analyze the reactor effluents. The trace of the MS profile at $m/z = 30$, relating to both NO(g) and NO_2(g), is shown in Fig. 2 during a series of lean-rich sequences at 300 °C and in the presence of 4% water. The reference levels of the signal were also collected at the end of the experiment by saturating the trap and then by removing the NO from the feed (corresponding to no NO*x* being present). Note that the level at $m/z = 30$ measured after totally removing the NO*x* from the feed did not go back to the zero value that was obtained during the signal zeroing of the MS (i.e. MS isolated). Other experiments (not shown) revealed that one isotope of CO (i.e. $^{12}C^{18}O$) was responsible for this remaining signal. The CO and CO_2 signals obtained from the IR gas-cell were used to correct the MS signal at $m/z = 30$, which thus only corresponded to NO*x* (NO and NO_2). This enabled calculating accurately the NO conversion and NO*x* trapped.

The signals of NO_2 at $m/z = 30$ and 46 were also calibrated and the intensity at the latter value was found to be ca. 10% of that at the former. It can therefore be approximated that the m/z signal observed at $m/z = 30$ (corrected for the $^{12}C^{18}O$ contribution) was equal to the concentration of NO*x* = NO + NO_2.

Complementary data obtained using the chemiluminescence cell indicated that for all the experimental conditions used, the NO*x* concentration value measured after trap saturation did not reach that of the inlet. This indicated that there was a contribution of direct reduction of NO to N_2 and/or N_2O due to the presence of CO and H_2 in the lean feed (via selective catalytic reduction, SCR). The SCR led to a reduction of the NO inlet concentration by about 4–6%.

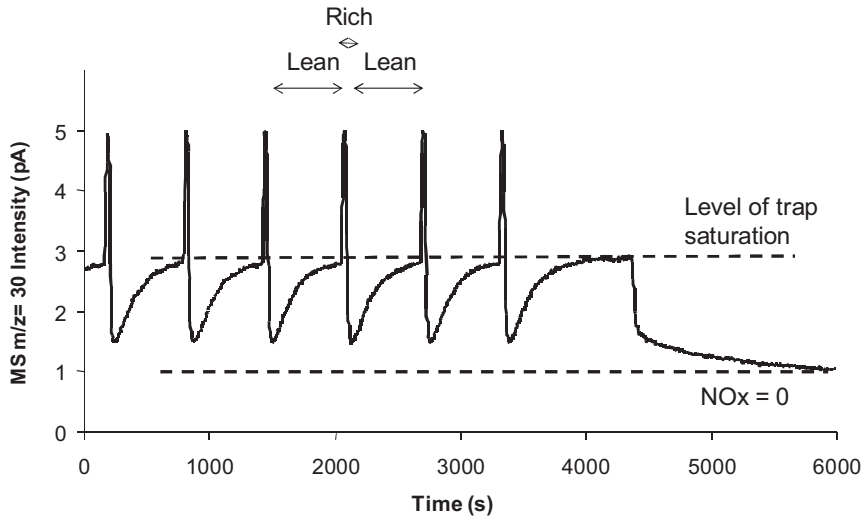

Fig. 2. Typical mass spectrometer profile of $m/z = 30$, relating mostly to NO(g) and NO_2(g) during a series of lean-rich sequences. The reference levels (dotted lines) of the signal were collected at the end of the experiment by saturating the trap and then removing the NO from the feed. The lean-rich cycling presented here was collected at 300 °C and under 4% water.

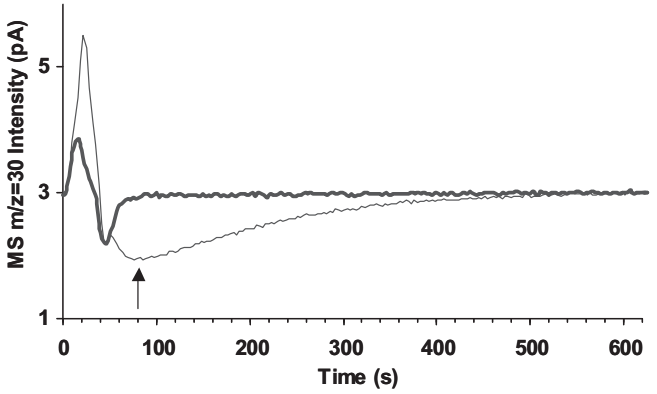

Fig. 3. Typical mass spectrometer profile of $m/z = 30$, corresponding to NO(g) and NO_2(g) during one rich-lean cycle. The rich-period spans over the 0–30 s period, while the lean period spans over the 30–630 s period. The thick line corresponds to the signal obtained over an empty reactor, while the thin dotted line corresponds to the signal obtained over the commercial NSR material. $T = 300\,^{\circ}C$. 4% water. (The point indicated by an arrow was used as reference point for the IR analysis).

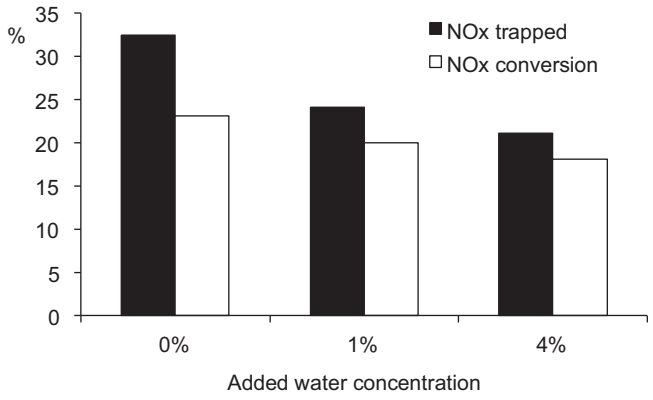

Fig. 4. Effect of the concentration of added water on the proportion of NO*x* stored (calculated over the lean period) and NO*x* conversion (calculated over the full cycle = lean + rich) derived from the MS analysis. $T = 300\,^{\circ}C$.

The MS data shown in Fig. 2 are consistent with the activity of typical NSR materials. The standard deviation of the NO*x* conversion was less than 5% over the five last lean-rich cycles. A strong release of NO*x* can be observed during the rich phase, which is better seen in the plot given in Fig. 3 that displays only one full cycle. The initial 30 s corresponded to the rich period, while the remaining 10 min corresponded to the lean phase. Due to a difference of dead-volume between the IR reactor line and that of the by-pass, a wave-like signal can be observed upon switching feed (see Fig. 3, thick line, for the signal change in the absence of any NSR sample). Each individual switching event resulted in a wave-like perturbation lasting about 30 s. The areas of the upper and lower waves exactly cancelled each other upon integrating over the full cycle and therefore did not introduce any experimental artifact in the calculation of the conversion. On the contrary, the calculation of the NO*x* trapped value (which only regarded the lean period) required correcting for this artifact, by subtracting the corresponding area obtained during a blank experiment (i.e. realized with no sample).

The time indicated by an arrow on Fig. 3 was that used to obtain the reference spectrum for the calculation of the IR absorbance spectra. This corresponded to the point of lowest NO*x*(g) concentration in the gas-phase at the beginning of the lean period, about 1 min after switching the 6-way valve to select the lean phase. This delay had to be used because of the time dispersion introduced by the cell and tubing dead-volume.

The proportion of NO*x* trapped over the lean-period at $300\,^{\circ}C$ under various concentrations of added water is reported in Fig. 4. Water had clearly a detrimental effect in the present case, as the NO*x* trapped decreased from 32.5% to 21% when the water content added to the feed increased from 0 to 4%. Experiments carried out with higher water concentrations (up to 10% – not shown here) did not lead to significant differences with respect to what observed at 4%. A similar decrease was observed for the NO*x* conversion with increasing water content. For each water concentration the proportion of NO*x* conversion was lower than that of NO*x* trapped, indicating that a significant fraction of NO*x* stored was then released without being reduced. The dry feed led to the largest difference between NO*x* stored and converted. This suggests that for a high amount of stored NO*x* their reduction is kinetically controlled or that water is actually beneficial for reducing NO*x*, possibly due to H_2 formation through the water–gas shift during the rich phase. Therefore, water appears to have a complex effect on NSR activity: on the one hand it hindered NO*x* storage and, on the other hand, it facilitated NO*x* reduction.

3.2. Operando spectroscopic results

A spectrum of the NSR material after activation at $600\,^{\circ}C$ was collected at $300\,^{\circ}C$ under the rich feed and 4% of added water just before starting the NSR cycles at the same temperature (Fig. 5a). The transmitted intensity below 1000 cm^{-1} was essentially nil because of the absorption by the various oxides present in the NSR material. The bands around 2360 cm^{-1} and those between 3750 and 3500 cm^{-1} were mainly due to the CO_2 present in the feed as well as ambient CO_2. The bands due to surface hydroxyl group stretching (region 3800–3000 cm^{-1}) were weak, despite the high water concentration present. The strong band at 1460 cm^{-1} was assigned to ionic carbonate species [36,37]. The carbonates presenting an IR band at this wavenumber are highly symmetric (i.e. D_{3h} space group) typical of large ionic crystals, hence the denomination "bulk-like species" sometimes used. This band at 1460 cm^{-1} is actually doubly degenerated and split into a doublet centered around 1460 cm^{-1} when the D_{3h} symmetry is lost. Several other ill-defined bands could be observed on either side of the 1460 cm^{-1} band and were assigned to ionic $BaCO_3$ species or to covalent carbonates, that may present a C_{2v} symmetry, such as bidentate and bridged surface species [38]. A typical spectrum obtained at the end of the lean period is also reported on the same figure (Fig. 5b). It is striking that the IR spectrum remained mostly unaffected, as carbonates remained the main sorbed species, most likely because of the overwhelming gas-phase concentration of CO_2 (10%) as

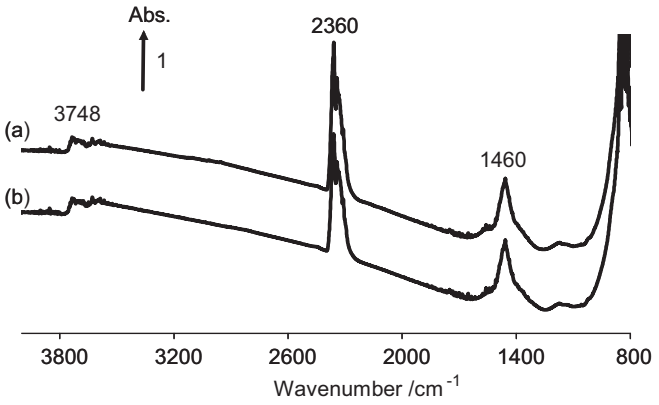

Fig. 5. (a) FTIR in situ spectrum at $300\,^{\circ}C$ under the rich phase feed with 4% of added water over the activated commercial NSR material. (b) Corresponding spectrum obtained at the end of the 10 min lean-phase. A spectrum obtained over the empty reaction cell was used as background to calculate the absorbance (the spectra were offset for the sake of clarity).

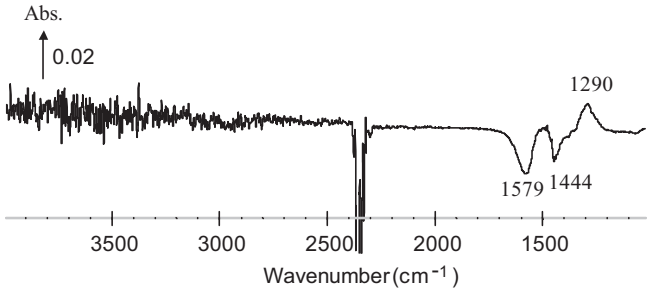

Fig. 6. FTIR in situ spectrum obtained over the activated commercial NSR material at 300 °C after 10 min under the lean phase feed comprising 4% water. A spectrum obtained over the same sample at the same temperature after 1 min in the lean phase was used as background to calculate the absorbance.

compared to that of NO*x* (i.e. the maximum NO*x* concentration was 180 ppm).

The minute changes of the IR spectrum of the NSR material after 10 min in the lean-phase were evidenced by difference spectra (Fig. 6), using as a reference the spectrum collected after 1 min in the lean-phase (see Section 3.1 and Fig. 3 for explanation). The smallness of the IR band changes observed during the lean period can be appreciated using the absorbance scales shown in Figs. 5 and 6; e.g. the band appearing at 1290 cm^{-1} (Fig. 6) had a 50-fold lower intensity than the ionic carbonate band at 1460 cm^{-1} (Fig. 5). It must be stressed that no significant changes were noted in the hydroxyl stretching region (3800–3000 cm^{-1}) (Fig. 6), therefore, it can be concluded that the trapping of NO*x* over hydroxyl groups was negligible.

Changes were only observed in the 1700–1200 cm^{-1} region, which is zoomed in Fig. 7. The positive broad band gradually appearing in the range 1350–1200 cm^{-1}, with a main peak at 1290 cm^{-1}, can be assigned to a large distribution of surface NO*x* species, typical of covalent nitrates species for which N–O bonds are not equivalent [39]. These covalent surface species can be adsorbed on the Ba, Mg, Ce, Zr or Al-based oxide phases with different coordination modes, e.g. monodentate and/or bidentate. It has been proposed that bands in this region could be assigned to dispersed monomeric or dimeric barium nitrate species, which are *de facto* also considered as surface species [12]. There should be for all these (split) bands a corresponding positive band at a higher wavenumber value (i.e. ca. 1560–1410 cm^{-1}) such that the average of the two wavenumbers equates the wavenumber of bulk ionic (D_{3h}) nitrates, which is ca. 1380 cm^{-1}. Unfortunately, the expected

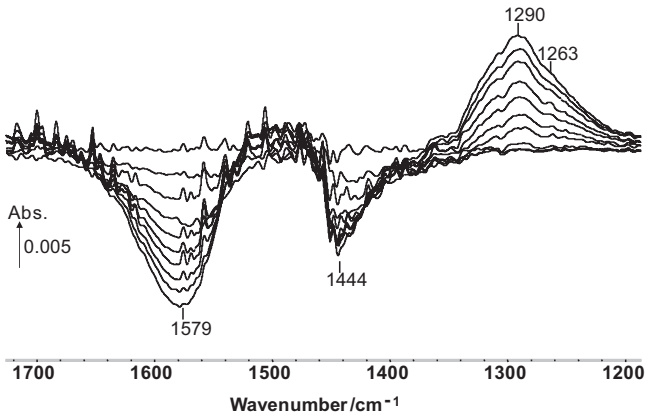

Fig. 7. FTIR in situ spectra obtained over the activated commercial NSR material at 300 °C under the lean phase feed comprising 4% water. A spectrum obtained over the same sample at the same temperature after 1 min in the lean phase was used as background to calculate the absorbance. The spectra were recorded using a 1 min interval.

high wavenumber component of the vibration spectrum of these surface nitrate species falls in the region of the signal associated with ionic carbonate species (centred at ~1450 cm^{-1}) and negative bands around 1444 and 1579 cm^{-1} were actually observed in this region. This observation can be rationalized by the fact that carbonates were being replaced by nitrates, leading to an overall decrease of the IR intensity in this region because of the higher molar absorption coefficient of carbonates as compared to nitrates.

The negative band around 1444 cm^{-1} corresponded to ionic polydentate and monodentate carbonates, while the strong negative band at around 1579 cm^{-1} can be assigned to covalent carbonates species, most likely being displaced by the covalent nitrate associated with the band at 1290 cm^{-1} discussed above. The leaving carbonate at 1579 cm^{-1} should also exhibit a band located at about 1320 cm^{-1}, barely visible because it falls in the region where the bands of ionic and covalent nitrate species are expected to grow. In fact this competition between species coordinated on the same sites affects the shape of the spectra around 1340 cm^{-1}. A precise decomposition of these various carbonate and nitrate bands was impossible, since many different types of surface species (mono, di and multi-coordinated species) are expected to co-exist on each of the oxide present, each of those likely presenting various types of surface sites. This explains the broad ill-defined shape of the 1579 cm^{-1} carbonate band and 1290 cm^{-1} nitrate band. Note that the presence of nitrite species was not observed at this temperature over this material under these conditions, while those were clearly observed at 100 and 200 °C [40], in agreement with previous studies on Ba-based materials [41].

To support the model discussed in the above-paragraph, the IR intensity of the surface nitrates band at 1290 cm^{-1} was plotted versus that of the band of the disappearing surface carbonates at 1579 cm^{-1} during the 10 min lean-phase. This was carried out for various water contents in the feed and in all cases a near-perfect linear correlation was obtained (Fig. 8). This observation is consistent with our model stating that the surface nitrates displaced a stoichiometric amount of surface carbonates during the duration of the lean-phase.

In conclusion, the evolution of the IR spectra of the NSR sample during the lean-phase (Figs. 6 and 7) can be rationalized as follow:

i. Ionic and covalent carbonates species are being replaced by the corresponding ionic and covalent nitrates.
ii. The low-wavenumber band of covalent nitrates (located at 1290 cm^{-1}) and high-wavenumber band of covalent carbonates (located at 1579 cm^{-1}) are the only bands that are not overlapping with those of the other species and can be clearly monitored and quantified.
iii. In the central region (comprised between 1290 and 1579 cm^{-1}) the signals of ionic nitrates and carbonates are overlapping and partially compensating each other, as well as the (high-wavenumber) stretching band of covalent nitrates and (low-wavenumber) stretching band of covalent carbonates.

3.3. *Effect of water on the IR spectrum*

The kinetic results discussed in Section 3.1 showed that increasing concentrations of steam led to a limited but noticeable decrease of the NO*x* conversion (Fig. 4). This was associated with a decrease of the quantity of NO*x* stored during the lean-phase (see Fig. 4 and Table 2). The comparison of the IR spectra collected at the end of the lean-phase under various concentrations of water shows that the presence of water reduced the storage of NO*x* as surface species (Fig. 9), in agreement with the results afore-mentioned. In particular, a band observed at 1251 cm^{-1} was markedly attenuated in the presence of 4% water, while being clearly visible at lower steam pressure. These results are consistent with those reported by Epling

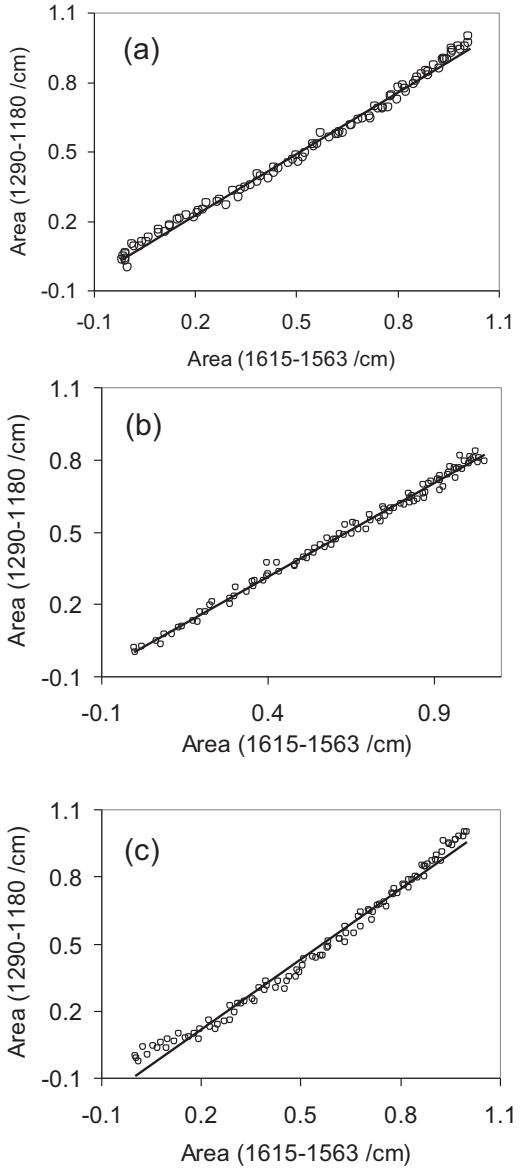

Fig. 8. IR intensity of the band appearing at 1290 cm^{-1} versus that of the band disappearing at 1579 cm^{-1} during the 10 min lean-phase for various added water content of the feed: (a) 0%, (b) 1% and (c) 4% water. The signals were normalized between 0 and 1 for the sake of clarity.

et al. obtained over other NSR materials, for which at least two types of sorption sites were inferred [42]. Consistent results were also reported by some of us earlier, where the species removed by the presence of water were assigned to weakly bound surface nitrates adsorbed on alumina [43].

The 1251 cm^{-1} component is associated with a positive band at ca. 1540 cm^{-1} that is also only detected when no water is added to the flow (Fig. 9), both bands being typical of surface aluminum nitrates. In the present case, it cannot be excluded that the other

Table 2
NO*x* storage capacity of the commercial material at 300 °C under various concentrations of water. Note that the material was recovered from a monolith and was therefore diluted in the other components of the wash-coat.

Water content (%)	Storage capacity (μmol g^{-1})
0	36.2
1	28.0
4	24.6

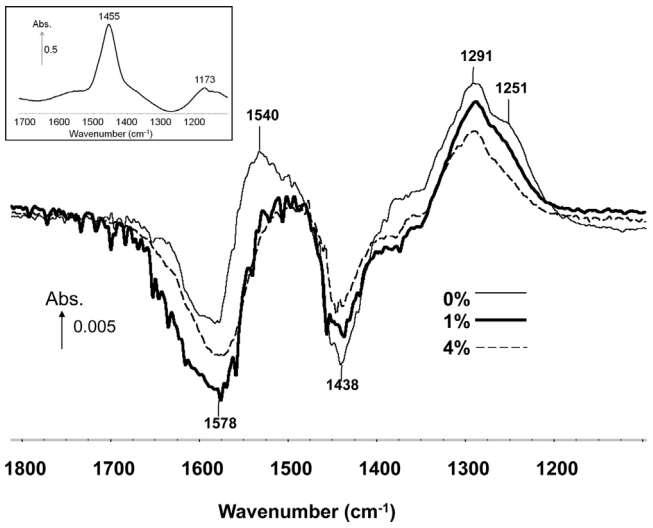

Fig. 9. FTIR in situ spectra obtained over the activated commercial NSR material at 300 °C after 10 min in the lean phase feed comprising various water concentrations. A spectrum obtained after 1 min in the lean phase was used as background to calculate the absorbance. The reference spectrum recorded at the beginning of the lean-phase is given in the insert.

oxides present contributed to this band, albeit to a limited extent since alumina was the most abundant oxide in our NSR sample. It is more difficult to draw any conclusion regarding the ionic nitrates, because of the strong overlapping of the IR bands of ionic species with those of covalent species. However, since the storage on covalent sites is negligible as compared to that on ionic site (vide infra, next section), it must therefore be concluded that the storage on ionic sites (that determines storage of the whole material) was also somehow affected by the presence of water.

3.4. Contribution of the surface nitrates to the storage at which 1% of water

The contribution of surface nitrates on the overall storage capacity of the sample was evaluated using an extended storage period of 120 min (Fig. 10). The trapping of NO*x*(g) was over after about 30 min, while the IR signal of covalent nitrates had only reached about 50% of its final value. This observation indicates that the contribution of covalent nitrates was actually negligible in the overall storage capacity.

This conclusion is also confirmed by the comparison of the missing gas-phase NO*x*(g) signal (Fig. 11) and that of the derivative of

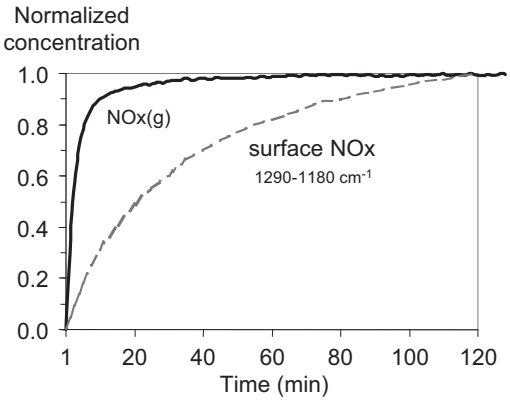

Fig. 10. Comparison of the NO*x* concentration in the reactor effluent (determined from the chemiluminescence signal) during a long lean period and the IR signal of the surface NO*x* species measured over the 1290–1180 cm^{-1} range (1% added water).

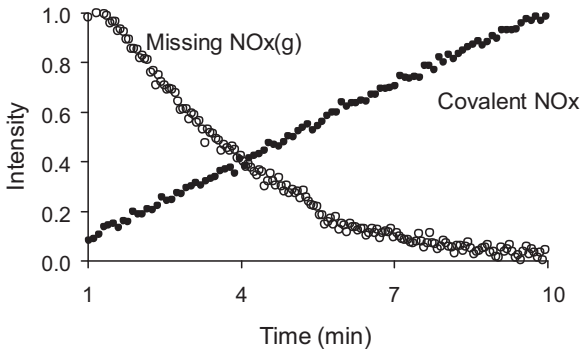

Fig. 11. Missing NO*x* concentration in the reactor effluent (determined with the MS) and the IR signal of the covalent NO*x* species measured over the 1290–1180 cm^{-1} range in the 1–10 min lean-period (normalized data) (1% added water).

the covalent nitrate concentration over the 10 min lean-period, as explained now. The number of moles of nitrates trapped over the sample at a time t is proportional to the integral of the missing NO*x*(g) concentration between the start of the lean-period ($t = 0$ was taken at the minimum of the NO*x*(g) concentration) and the time t (Eq. (3)). The IR signal of these nitrates is proportional to the amount of these trapped species (Eq. (4)). This is based on the safe assumption that the molar absorption coefficient does not depend on the nitrate concentration. Taking the derivative form of Eq. (3) and combining with Eq. (4), it appears that the derivative of the IR signal of the nitrate species responsible for the storage should be proportional to the missing NO*x* concentration (Eq. (5)).

$$\text{Trapped NO}x(t) \alpha \int_0^t \text{missing NO}x(\text{g})(\tau)\text{d}\tau \quad (3)$$

$$\text{IR}(t) \alpha \text{ trapped NO}x(t) \quad (4)$$

$$\frac{\text{d IR}(t)}{\text{dt}} \alpha \text{ missing NO}x(t) \quad (5)$$

Since the signal of covalent nitrates varies monotonously over the first 10 min of the lean-period (Fig. 11), the corresponding derivative is a constant. However, the plot representing the missing NO*x*(g) over the same period of time is clearly not a constant (Fig. 11). Therefore, the covalent NO*x* are confirmed as not being the main form under which the NO*x* were trapped on our material.

3.5. Correlation of the IR signal of ionic species and the NOx trapped

The overlapping of bands due to ionic and covalent carbonates and nitrate species makes a complete signal deconvolution worthless. The variation of the IR intensity around the negative band at 1438 cm^{-1} (Fig. 9) clearly relates to (i) the removal of ionic carbonates absorbing at ca. 1450 cm^{-1}, (ii) the removal of covalent carbonates absorbing at ca. 1342 cm^{-1} (see Section 3.2), (iii) the formation of ionic nitrates absorbing at ca. 1380 cm^{-1} and (iv) the formation of covalent nitrates absorbing at ca. 1450 cm^{-1} (see Section 3.2). Interestingly, the variation of the IR signal of covalent nitrates and covalent carbonates is linear over the 10 min lean period (see Figs. 11 and 8). Therefore, the derivative of the signals of covalent species should each give a constant value over the 10 min lean-period.

A function representing only the difference of the signals of ionic nitrates stored and ionic carbonates released should thus be obtained by taking the derivative (as to get rid of the monotonous contribution from the covalent species) of the bands in the region associated with ionic species. Therefore, a band intensity was

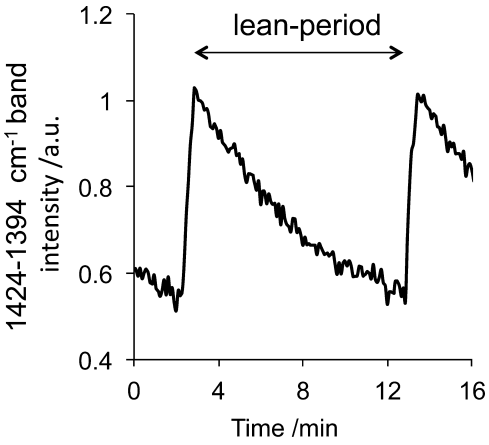

Fig. 12. Intensity of the IR signal of ionic/bulk species integrated over the spectral region 1424–1394 cm^{-1}. The origin of the timescale is arbitrary (1% added water).

measured in the spectral region 1424–1394 cm^{-1}, which is in between the position of ionic/bulk carbonates (1460 cm^{-1}) and that of ionic/bulk nitrates (1380 cm^{-1}). The band intensity decreased during the lean period, showing that carbonate removed affected more the signal that the added nitrates (Fig. 12). The decaying IR signal was fitted to a power-law function and derived, before being normalized to compare its variation with that of the missing NO*x* signal.

The normalized derivative curve of the ionic/bulk species IR band was similar to the line representing the missing NO*x* (Fig. 13); the minor differences being due to errors introduced by the spread of the gas-phase signal due to dead-volumes and the minor storage of NO*x* as surface covalent species. In view of Eq. (5), the trapping properties of this commercial NSR material can thus be related to the ionic species, i.e. the replacement of ionic carbonate species with ionic nitrate species.

A calculation based on the concentration of Ba in our sample and that of NO*x* trapped (see Table 2) revealed that the total number of stored nitrates never went beyond 10% of the total capacity of the Ba sites (assuming each Ba can store two nitrate ions). This stresses that only a minor fraction of the Ba sites were effectively used under our reaction conditions, possibly only the outer surface shell of Ba carbonate

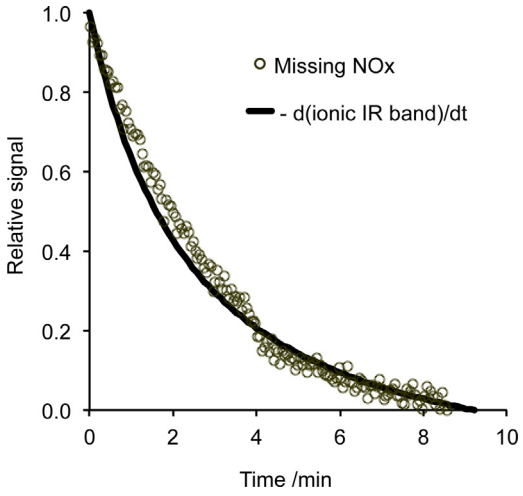

Fig. 13. Comparison of the normalized missing NO*x* concentration in the reactor effluent determined by mass spectrometry and the opposite of the derivative of the IR signal of the ionic/bulk species reported in Fig. 12. The derivative was calculated by deriving a fitting curve (power-law based) of the ionic/bulk IR signal.

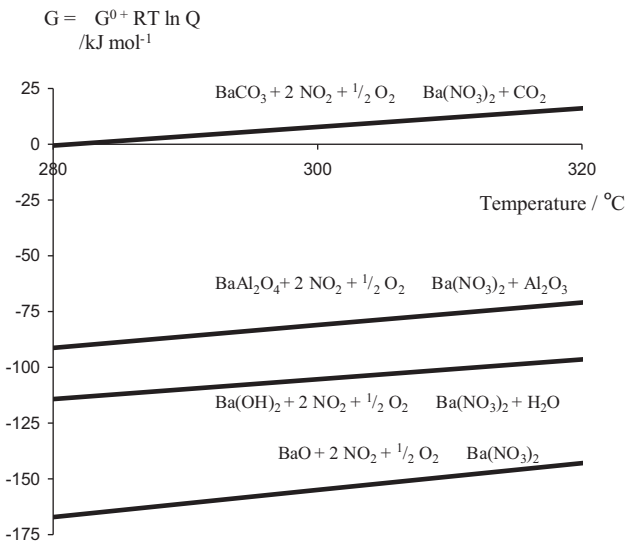

Fig. 14. Gibbs free energy of reaction relating to the nitration of various barium phases with NO_2. The actual values of NO_2, O_2, CO_2 and water in the reactor effluent were used to calculate the reaction quotient Q and determine the corresponding variation of Gibbs free energy.

particles. Of course different reaction conditions will likely affect these results: longer lean periods could let reaching a larger amount of storage sites, whereas a faster kinetics might result in a greater relevance of covalent species for NO*x* storage.

3.6. Possible nature of the trapping sites

The exact nature of the covalent species observed cannot be determined solely based on this IR work. The nature of the metal ion and phase over which the nitrates/carbonates are adsorbed is unclear, as well as the bonding mode (mono, bi, multi dentate). Nevertheless, it is likely that the covalent species are mostly located at the surface of the oxides used as support such as alumina and ceria. That is coherent with the observed wavenumbers.

Similarly, the nature of the ionic species exchanging is unclear. While the NSR material contains a large proportion of barium carbonate (identified by the band centered at 1460 cm^{-1}, Fig. 5a and b), it is likely that most of these carbonates are bulk species and do not participate to the storage. As a matter of fact, thermodynamic calculation revealed that at our reaction temperature (i.e. 300 °C) the nitration of barium carbonate is not spontaneous (as $\Delta G > 0$, Fig. 14) under our reaction conditions (the exact values of gas composition at the reactor exit were used to calculate the reaction quotient Q). This is in contrast to the other phases considered, i.e. barium aluminate, oxide and hydroxide, for which the nitration is spontaneous under our reaction conditions (Fig. 14).

This calculation refers of course to ideal bulk solids. It is possible that (i) distorted nanocrystals of barium carbonate, (ii) surface sites of large barium carbonate particles (iii) Ba carbonate doped by any one of the other elements present in the material and/or (iv) barium carbonate monomers could possibly get nitrated under our reaction conditions. The IR spectrum of the corresponding ionic species would probably be somewhat different from that of the ideal bulk ionic carbonate absorbing at 1460 cm^{-1}. Because it was not possible to decompose the IR spectrum obtained here and in view of the complexity of the washcoated material the exchange of ionic species observed in the 1424–1394 cm^{-1} region (Fig. 12) is certainly related to such ionic-like species and not "ideal" bulk ionic barium carbonate. The splitting of the degenerated band at 1460 cm^{-1} would yet be minor, so that these bands did not merge with that of the covalent adsorbed on alumina and other oxides

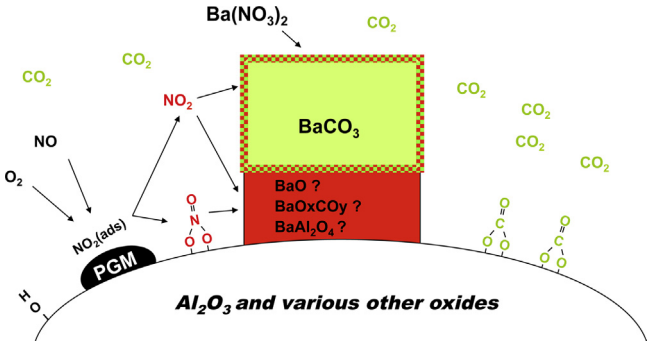

Fig. 15. Schematic representation of the storage process over a commercial NO*x*-storage-reduction material at the end of the lean-period under realistic conditions. (PGM = platinum group metal particle). The main nitrate storage process occurs over ionic-like sites through carbonate replacement, but this is unlikely to involve very stable bulk carbonates in $BaCO_3$. The storage phase remains mostly as a carbonate phase (>90%) during the lean-period. The sorption of NO*x* on hydroxyl sites and surface covalent sites is negligible as compared to that over the ionic sites. Trapping as ionic species onto barium aluminate or barium oxide phase (on oxide sites or/and by carbonate replacement) and the other elements present such as Mg, Ce, Sr and Cs is also possible.

present. It is also possible that some other elements present (such as Mg, Ce, Sr, Cs) also contributed to some extent to the formation of the ionic species. A schematic representation of the storage features of our commercial NSR material is given in Fig. 15.

4. Conclusions

A commercial NO*x*-storage-reduction material was investigated by combined IR and kinetic analysis using a low-volume *operando* cell under representative conditions. Water appeared to have a complex effect on NSR activity: on the one hand it hindered NO*x* storage and, on the other hand, it facilitated NO*x* reduction. The data showed that ionic and covalent carbonates species were replaced by the corresponding ionic and covalent nitrates. Despite partial or total band overlapping of the IR bands of these species, several conclusions could be derived on the relevance of the species present to the NSR process and their quantitative contribution. The contribution to NO*x* trapping of covalent species was negligible as compared to that of ionic species over this commercial sample. The involvement of hydroxyl groups in the trapping of NO*x* could also be neglected. The large NO*x* uptake observed could instead be essentially related to the replacement of ionic carbonates by ionic nitrates, although it is unlikely that bulk sites of large particles of barium carbonates were involved, because of thermodynamic limitations. The nitration of the bulk carbonate sites always remained low, i.e. <10% in all cases. It is also possible that some other elements present (such as Mg, Ce, Sr, Cs) contributed to some extent to the formation of the ionic species.

In a more general perspective, the present work demonstrates the power of *operando* studies of complex NSR materials by combined FTIR and on-line mass spectrometry/chemiluminescence analysis using realistic experimental conditions (e.g. high proportion of water and CO_2 as well as complex gas mixtures).

Acknowledgments

The French General Directorate for Enterprises (DGCIS) is acknowledged for the financial support provided to the present study through the collaborative project "OSCCAR'NOx".

References

[1] R. Burch, J.P. Breen, F.C. Meunier, Appl. Catal. B: Environ. 39 (2002) 283.

[2] N. Takahashi, H. Shinjoh, T. Iijima, T. Suzuki, K. Yamazaki, K. Yokota, H. Suzuki, N. Miyoshi, S. Matsumoto, T. Tanizawa, T. Tanaka, S. Tateishi, K. Kasahara, Catal. Today 27 (1996) 63.
[3] S. Roy, A. Baiker, Chem. Rev. 109 (2009) 4054.
[4] P. Granger, V.I. Parvulescu, Chem. Rev. 111 (2011) 3155.
[5] W.S. Epling, L.E. Campbell, A. Yezerets, N.W. Currier, J.E. Parks, Catal. Rev. Sci. Eng. 46 (2004) 163.
[6] J.P. Breen, C. Rioche, R. Burch, C. Hardacre, F.C. Meunier, Appl. Catal. B: Environ. 72 (2007) 178.
[7] N.W. Cant, M.J. Patterson, Catal. Today 73 (2002) 271.
[8] A. Casapu, J.D. Grunwaldt, M. Maciejewski, F. Krumeich, A. Baiker, M. Wittrock, S. Eckhoff, Appl. Catal. B: Environ. 78 (2008) 288.
[9] S. Salasc, M. Skoglundh, E. Fridell, Appl. Catal. B: Environ. 36 (2002) 145.
[10] I. Nova, L. Lietti, L. Castoldi, E. Tronconi, P. Forzatti, J. Catal. 239 (2006) 244.
[11] L. Olsson, E. Fridell, J. Catal. 210 (2002) 340.
[12] J. Szanyi, J.H. Kwak, J. Hanson, C.M. Wang, T. Szailer, C.H.F. Peden, J. Phys. Chem. B 109 (2005) 7339.
[13] J.H. Kwak, D. Mei, C.-W. Yi, D.H. Kim, C.H.F. Peden, L.F. Allard, J. Szanyi, J. Catal. 261 (2009) 17.
[14] T. Lesage, C. Verrier, P. Bazin, J. Saussey, S. Malo, C. Hedouin, G. Blanchard, M. Daturi, Top. Catal. 30–31 (2004) 31.
[15] L. Masdrag, X. Courtois, F. Can, D. Duprez, Appl. Catal. B: Environ. 146 (2014) 12.
[16] Z. Say, E.I. Vovk, V.I. Bukhtiyarov, E. Ozensoy, Appl. Catal. B: Environ. 142 (2013) 89.
[17] J. Szanyi, C.W. Yi, K. Mudiyanselage, J.H. Kwak, Topic. Catal. 56 (2013) 1420.
[18] Y. Zhang, M. Meng, F. Dai, T. Ding, R. You, J. Phys. Chem. C 117 (2013) 23691.
[19] L. Wang, R. Ran, X.D. Wu, M. Li, D. Weng, J. Rare Earths 31 (2013) 1074.
[20] B. Pereda-Ayo, J.A. Botas-Echevarria, J. Gonzalez-Casablanca, M.P. González-Marcosa, J.R. González-Velasco, Catal. Today 216 (2013) 50.
[21] K.-I. Shimizu, Y. Saito, T. Nobukawa, N. Miyoshi, A. Satsuma, Catal. Today 139 (2008) 24.
[22] I. Malpartida, M.O. Guerrero-Pérez, M.C. Herrera, M.A. Larrubia, L.J. Alemany, Catal. Today 126 (2007) 162.
[23] T. Lesage, J. Saussey, S. Malo, M. Hervieu, C. Hedouin, G. Blanchard, M. Daturi, Appl. Catal. B: Environ. 72 (2007) 166.
[24] J. Szanyi, J.H. Kwak, R.J. Chimentao, C.H.F. Peden, J. Phys. Chem. B 111 (2007) 2661.
[25] V. Dal Santo, C. Dossi, A. Fusi, R. Psaro, C. Mondelli, S. Recchia, Talanta 66 (2005) 674.
[26] A. Urakawa, N. Maeda, A. Baiker, Angew. Chem. Int. Ed. 47 (2008) 9256.
[27] T. Lesage, C. Verrier, P. Bazin, J. Saussey, M. Daturi, Phys. Chem. Chem. Phys. 5 (2003) 4435.
[28] C.G. Visconti, L. Lietti, F. Manenti, M. Daturi, M. Corbetta, S. Pierucci, P. Forzatti, Top. Catal. 56 (2013) 311.
[29] F.C. Meunier, A. Goguet, S. Shekhtman, D. Rooney, H. Daly, Appl. Catal. A: Gen. 340 (2008) 196.
[30] H. Li, M. Rivallan, F. Thibault-Starzyk, A. Travert, F.C. Meunier, Phys. Chem. Chem. Phys. 15 (2013) 7321.
[31] F.C. Meunier, Chem. Soc. Rev. 39 (2010) 4602.
[32] A. Carías-Henriquez, S. Pietrzyk, C. Dujardin, Catal. Today 205 (2013) 134.
[33] L.F. Bobadilla, O. Marie, P. Bazin, M. Daturi, Catal. Today 205 (2013) 24.
[34] W.O. Siegl, R.H. Hammerle, H.M. Herrmann, B.W. Wenclawiak, B. Luers-Jongen, Atmos. Environ. 33 (1999) 797.
[35] H. Ogawa, T. Li, Int. J. Eng. Res. 12 (2011) 30.
[36] A.D. Cross, Introduction to Practical IR Spectroscopy, Buttersworth, London, 1964.
[37] N.B. Colthup, L.H. Daly, S.E. Wiberley, Introduction to Infrared and Raman Spectroscopy, Academic Press, Boston, 1990.
[38] K. Nakamoto, Infrared and Raman Spectra of Inorganic and Coordination Compounds, 4th ed., Wiley-Interscience, New York, 1986.
[39] K.I. Hadjiivanov, Catal. Rev. Sci. Eng. 42 (2000) 71.
[40] J. Dupré, P. Bazin, O. Marie, M. Daturi, X. Jeandel, F.C. Meunier (2014), in preparation.
[41] L. Lietti, M. Daturi, V. Blasin-Aubé, G. Ghiotti, F. Prinetto, P. Forzatti, ChemCatChem 4 (2012) 55.
[42] W.S. Epling, J.E. Parks, G.C. Campbell, A. Yezerets, N.W. Currier, L.E. Campbell, Catal. Today 96 (2004) 21.
[43] B.I. Mosqueda-Jimenez, A. Lahougue, P. Bazin, V. Harle, G. Blanchard, A. Sassi, M. Daturi, Catal. Today 119 (2007) 73.